https://doi.org/10.5194/egusphere-2022-1483
Preprint. Discussion started: 4 January 2023

Choice of Forecast Scenario Impacts the Carbon Allocation at the Same Global Warming Levels

Lee de Mora[1], Ranjini Swaminathan[2], Richard P. Allan[2], Jeremy Blackford[1], Douglas I. Kelley [3], Phil Harris[3], Chris D. Jones[4], Colin G. Jones[5], Spencer Liddicoat[4], Robert J. Parker[6,7], Tristan Quaife[2], Jeremy Walton[4], and Andrew Yool[8]

[1]Plymouth Marine Laboratory, Plymouth, PL1 3DH
[2]National Centre for Earth Observation and Department of Meteorology, University of Reading, Reading, UK
[3]UK Centre for Ecology & Hydrology, Wallingford, Oxfordshire, OX10 8BB, UK
[4]Met Office Hadley Centre for Climate Science and Services, Exeter, EX1 3PB, UK
[5]National Centre for Atmospheric Science, UK, and School of Earth and Environment, University of Leeds, Leeds, UK
[6]National Centre for Earth Observation, Space Park Leicester, University of Leicester, Leicester, UK
[7]Earth Observation Science, School of Physics and Astronomy, University of Leicester, UK
[8]National Oceanography Centre, European Way, Southampton, SO14 3ZH, UK

Correspondence: Lee de Mora (ledm@pml.ac.uk)

Abstract.

The anthropogenic carbon distribution between the atmosphere, land surface and ocean varies significantly with the choice of scenario for identical changes in mean global surface temperature. Moving to a lower CO_2 emissions scenario means that warming levels occur later, and with significantly less carbon in the three main carbon reservoirs. After 2°C of warming, the multi-model mean ocean allocation can be up to 3% different between scenarios, or 36 Pg in total with an even larger difference in some single model means. For the UKESM1 model, the difference between the minimum and maximum atmospheric fraction at the 2°C Global Warming Level (GWL) is 3.6%. This is equivalent to 50 Pg of additional carbon in the atmosphere, or the equivalent of five years of our current global total emissions.

In the lower CO_2 concentration scenarios, SSP1-1.9 and SSP1-2.6, the ocean fraction grows over time while the the land surface fraction remains constant. In the higher CO_2 concentration scenarios, SSP2-4.5, SSP3-7.0 and SSP5-8.5, the ocean fraction remains constant over time while the the land surface fraction decreases over time.

Higher equilibrium climate sensitivity (ECS) models reach the GWLs sooner, and with lower atmospheric CO_2 than lower sensitivity models. However, the choice of scenario has a much larger impact on the percentage carbon allocation at a given warming level than the individual model's ECS.

Keywords: Climate change, CMIP6, Earth System Models, Carbon Cycle, Carbon Allocation

1 Introduction

The Intergovernmental Panel on Climate Change (IPCC) Sixth Assessment Report (AR6) found that the global mean surface air temperature is 1.1°C warmer in the recent decade (2011-2020) compared to the pre-industrial era. They also concluded that

https://doi.org/10.5194/egusphere-2022-1483
Preprint. Discussion started: 4 January 2023

human activities have indisputably caused this warming (IPCC, 2021b). Anthropogenic greenhouse gases in the atmosphere, particularly carbon dioxide (CO_2), are the primary cause of this heating. In addition to warming the climate, this additional CO_2 affects other parts of the Earth system including vegetation change via carbon fertilisation, and ocean acidification.

The Earth system's carbon cycle centres around the exchange of carbon between the atmosphere, the land surface, the ocean and geological reserves, such as fossil fuels. Since the advent of the Industrial Revolution, carbon has effectively been transferred from the fossil fuel reservoir to the atmosphere via combustion for energy generation. From the atmosphere, the ocean absorbs anthropogenic carbon via gas transfer, and the land surface via primary production, while some CO_2 remains in the atmosphere. The instantaneous distribution of anthropogenic carbon between the atmosphere, ocean and land surface is known as carbon allocation, illustrated in fig. 1. Note that while in nature there is a flux of land carbon into the ocean via rivers between 0.45 ± 0.18 PgC yr^{-1} and 0.78 ± 0.41 PgC yr^{-1} Jacobson et al. (2007); Resplandy et al. (2018); Hauck et al. (2020), and a flux of fossil fuels directly into the ocean or land surface via for instance fossil fuel extraction (Roser and Ritchie, 2022), these are not generally included in CMIP6 models.

Projections of the ultimate fate of anthropogenic carbon are essential because its impact depends on its destination within the Earth system. In the atmosphere, anthropogenic carbon causes additional warming (Hansen et al., 1981). In the ocean, anthropogenic carbon can cause acidification (Caldeira and Wickett, 2003) or participate in primary production or sequestration (Schlunegger et al., 2019). On the land surface, carbon can allow enhanced primary production and subsequent carbon sequestration. Carbon may be a fuel source once converted into biomass (Burton et al., 2022; Sullivan et al., 2022), alter transpiration rates which impact flood and drought risk Ukkola et al. (2016) and worsen food quality and nutrient (Erda et al., 2005).

Earth System models are one of the main tools that we have to study the climatic impact of the combustion of fossil fuels and they are the only tool that we have to make forecasts of the future climate. The Sixth Coupled Model Inter-comparison Project (CMIP6) (Eyring et al., 2016) is the most recent in a series of global efforts to standardise, share and study Earth System Model simulations. CMIP6 is an international collaborative project which allows modelling groups from around the world to share their climate model output data. In order to participate in CMIP6, models must meet a certain set of standards for scientific model quality and data standardisation. This means that the model outputs must use a common format and meet the minimum quality requirements. These minimum quality requirements include a drift in the air-sea flux of CO_2 of less than 10 Pg century^{-1}, and a drift in the global volume mean ocean temperature of less than 0.1 degrees per year (Jones et al., 2011; Eyring et al., 2016; Yool et al., 2020).

As we are unable to predict the future anthropogenic climate drivers, multiple scenarios were proposed in the ScenarioMIP project to cover a wide range of potential futures. These ScenarioMIP scenarios expand upon the CMIP6 core simulations and multiple scenarios are available for modellers to use to generate simulations (O'Neill et al., 2016). We include the scenarios: SSP1-1.9, SSP1-2.6, SSP2-4.5, SSP3-7.0 and SSP5-8.5 (O'Neill et al., 2016; Riahi et al., 2017). These scenarios cover a wide range of possible futures, including sustainable development in the SSP1-1.9 and SSP1-2.6 scenarios. The "middle of the road" pathway in SSP2-4.5 extrapolates historic and current global development into the future with a medium radiative forcing by the end of the century. The regional rivalry scenario, SSP3-7.0, revives nationalism and regional conflicts, pushing global

https://doi.org/10.5194/egusphere-2022-1483
Preprint. Discussion started: 4 January 2023

issues into the background and resulting in higher emissions. Then finally, the enhanced fossil fuel development in SSP5-8.5 is a forecast with the highest feasible fossil fuel deployment and atmospheric CO_2 concentration.

Each model in CMIP6 has a different sensitivity to carbon. This means that for the same atmospheric CO_2 concentration, each model will warm by a different amount. A measure of how sensitive each model is to CO_2 is it's equilibrium climate sensitivity (ECS). The ECS is given in °Celsius and represents the long-term near-surface air temperature rise that is expected to result from a doubling of the atmospheric CO_2 concentration. The ECS is a good indicator for how rapidly a given model warms to a given GWL for a given CO_2 pathway. The most recent 5-95% assessed ECS range was between 2°C and 5°C, and the likely ECS range was 2.5 - 4°C, (Arias et al., 2021, TS6.). An alternative measure of sensitivity that is often used is the transient climate response to cumulative emissions of CO_2 (TCRE). The TCRE is the ratio of the globally averaged surface temperature change per unit of CO_2 emitted (Williams et al., 2020). The TCRE and ECS differ in that the TCRE is calculated while the heat distribution between the land, ocean and atmosphere is not yet at equilibrium. The wide spread of ECS and TCRE values in climate models is one of the causes of uncertainty on when the world is forecast to reach certain global warming levels. The "allowable emissions" that keep global temperature rise within Paris agreement targets are similarly impacted (Collection, 2015). This has been exacerbated in the latest round of CMIP, as the CMIP6 generation of ESMs has a broader range of sensitivities than previous generations. Several CMIP6 models have a stronger response to atmospheric carbon than any CMIP5 model, and many sit above the likely ECS range from Arias et al. (2021, TS6.).

Climate change policy can often focus on the climate at specific target years, like 2050 or 2100 (Collection, 2015). Instead of specific target years, we can alternatively use global warming levels (GWL), such as 2°C, 3°C or 4°C of warming relative to the pre-industrial period. The 2°C GWL is defined in the Paris Agreement (Collection, 2015) and thought to be a threshold for potentially dangerous climate change. The 3°C is close to the warming level that current nationally determined contributions could take us in the year 2100 with a median climate sensitivity. Finally, the 4°C GWT is a low likelihood but high impact outcome if climate sensitivity is higher than median values or emission reductions and climate policy breaks down. By investigating the system's behaviour at specific warming levels instead of target years we can reduce the impact of climate sensitivity and make policy relevant assessments while still exploiting the full ensemble of CMIP6 models.

The carbon allocation for CMIP6 projections at the year 2100 appears in (IPCC, 2021a, fig. SPM7). This figure shows that with increasing CO_2 concentrations scenarios, the atmospheric fraction (AF) at the year 2100 rises with increasing CO_2 concentrations. In SSP1-1.9, 30% of the carbon remains in the atmosphere in the year 2100, but in SSP5-8.5, that figure is 62%. However, it was not previously known what the behaviour will be at certain GWLs. The aim of this work is to investigate whether the distribution of carbon between the various reservoirs is impacted by the choice of scenario at these GWLs.

To investigate how much carbon allocation varies between different scenarios without the complexity of a multi-model ensemble, we focus on a single model: the first United Kingdom Earth System Model, UKESM1, which is labelled as UKESM1-0-LL in CMIP6. UKESM1 model was chosen as a focus model because it has a large ensemble, includes all the scenarios under investigation and several members of the authorship team contributed to the development of the UKESM1 model. From a single model we can also understand the processes controlling any changes better and look to see the level of time variability in the sinks due to internal model variability.

https://doi.org/10.5194/egusphere-2022-1483
Preprint. Discussion started: 4 January 2023

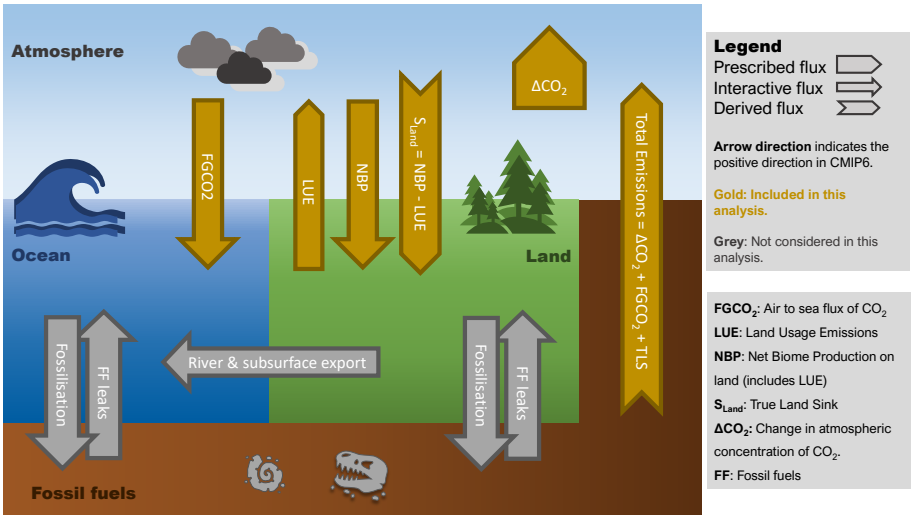

Figure 1. A simplified version of the Earth system carbon cycle. Interactive fluxes are shown as regular arrows, prescribed fluxes are shown as box arrows, and derived fluxes are shown as chevrons. The arrows in gold are considered in this analysis. Note that while in nature there is a flux of land carbon into the ocean via rivers, and there may be a flux of fossil fuels directly into the ocean or land surface via for instance fossil fuel extraction, these are not generally included the CMIP6 models we consider in this paper. CMIP6 models do not generally include these fluxes of land carbon into the ocean via rivers. There may be a flux of fossil fuels directly into the ocean or land surface via for instance fossil fuel extraction.

2 Methods

2.1 Carbon allocation calculation

We calculate the carbon allocation for the land, ocean and atmospheric reservoirs separately. On the land surface, the land carbon sink, S_{LAND} is derived from the global total net biome production (NBP) and the global total land use emissions (LUE). As NBP is defined as the difference between land sink and emissions from land use ($NBP = S_{LAND} - LUE$), then:

$$S_{LAND} = NBP + LUE \tag{1}$$

The NBP is an prognostic variable calculated by the models. We calculated the global total net biome production using the land area-weighted sum of the local NBP over the entire global land surface. It is defined as positive for fluxes into the land carbon store (Jones et al., 2016). From CMIP6 simulations, it is not possible to directly isolate the LUE and so these are taken from land use scenarios common across all models and all ensemble members following Liddicoat et al. (2021). Note that CMIP6 experiments expresses the LUE in units positive into the atmosphere, but the NBP in units positive into the land.

https://doi.org/10.5194/egusphere-2022-1483
Preprint. Discussion started: 4 January 2023

The ocean component of the carbon allocation is the total global sum of the air sea flux of CO_2, $FGCO_2$. We calculated this as the sum of the air-sea flux of CO_2 multiplied by the ocean area of each cell. This is typically expressed as an annual total, so the total cumulative flux is calculated as the cumulative sum of the global annual total fluxes along the time dimension.

In the atmosphere, the CO_2 concentration is provided in the scenario forcing from ScenarioMIP in units of parts per million (ppm). The total mass of the carbon in atmospheric CO_2, C_{atmos} is calculated by multiplying the concentration in ppm by a constant factor. This conversion factor is $1ppm$ of CO_2 is equivalent to 2.13 Pg C Myers (1983).

No matter how much carbon the land and ocean components absorb from the atmosphere, the atmospheric concentration of CO_2 will always strictly follow the prescribed atmospheric CO_2 concentrations of the forcing scenario. This means that anthropogenic emissions can be estimated for each model (Jones et al., 2013). The total anthropogenic emissions are the sum of the total carbon in the atmospheric CO_2 and the cumulative global total carbon dioxide flux into the sea and the true land sink.

$$Emissions = C_{atmos} + FGCO_2 + S_{LAND} \tag{2}$$

Mass balance emissions can only provide the fossil-fuel term, not the land-use term. Here, we take land-use emissions from the scenario, so they are not in balance with run-time model behaviour: this means that S_{LAND} is only an approximation.

2.2 Included Models

Our analysis used all models for which the following three variables were available as monthly averages over the time period 1850-2100: the near-surface atmospheric temperature (tas), the net biome productivity (nbp) and the air to sea flux of carbon dioxide (fgco2). We limited each model to only the first ten ensemble members for each scenario, and required at least one historical and future scenario pair for each ensemble member. The additional grid cell information and areal extent were also required for both land and sea grids. We excluded the entire ensemble member if any variables were absent, the time series was incomplete, or the data could not be made compliant with CMIP6 standards.

Modelling centres may contribute more than one ensemble member for each scenario to the Earth System Grid Federation (ESGF). For instance, the UKESM1 model produced 19 different variants for the historical experiment, each using slightly different initial conditions drawn from the pre-industrial control (piControl) simulation (Sellar et al., 2020). This generates an ensemble of variants which samples a wide range of the unforced variability simulated by the model. By spanning the range of internal (natural) variability simulated by the model, the mean of a single model ensemble can gives a more robust estimate of the forced climate change. Each modelling centre may choose which scenarios they simulate and how many ensemble members for each scenario. This means that there is wide variation in the number of ensemble members between models. To balance models with large ensembles against models with small ensembles, we used a “one model - one vote” weighting scheme. This means that each model was given equal weight in the final multi-model mean. In practice, each ensemble member of a given model was weighted inverse proportionally to the number of ensemble members that the model contributed. No effort was made to weigh the results regarding the model quality or historical performance. Individual component models can be used by

https://doi.org/10.5194/egusphere-2022-1483
Preprint. Discussion started: 4 January 2023

several modelling centres. For instance, the NEMO ocean circulation model may appear in several of the earth system models. This means that these models can not be treated as statistically independent.

Table 1 lists the contributing models, the number of ensemble members for each scenario, and each model's equilibrium climate sensitivity (ECS). The ECS is included here because it plays a first order role in how rapidly a given model reaches a given GWL for a given CO_2 pathway. We took the model ECS values from Zelinka et al. (2020), with the exceptions of CMCC-ESM2 (Lovato et al., 2022), and the NorESM2-MM, ACCESS-ESM1-5 and MPI-ESM1-2-LR models (Hausfather, 2022). All quoted values use the Gregory et al. (2004) method to calculate ECS. We assumed that the CanESM5-CanOE model's ECS value is the same value as the sibling CanESM5 model. This table also shows the weighted ECS for the contributing models for each scenarios. The weighted ECS is only weighted by the presence or absence of models, not the number of contributing ensemble members, reflecting the "one-model one-vote" weighting scheme described above. The SSP1-1.9 ensemble contains fewer models than the other scenarios, and includes both the CanESM5 and UKESM1 models, which have the highest ECS values of our CMIP6 stable of models. The spread of weighted ECS values between scenarios is small, ranging from 4.34 for SSP5-85 to 4.23 for SSP2-45. However, all of these ensemble means sit above the likely ECS range of 2.5°C - 4°C, and some of the individual models are even outside the 5-95% confidence band, 2°C and 5°C (Arias et al., 2021, TS6.) (Sherwood et al., 2020).

There are two CESM2 models and two CanESM5 models. These model pairs are likely only to have slight differences. In addition, several models may share contributing component models. For instance the NEMO model forms the marine circulation component in several models. While the models in the group are not statistically independent, it is beyond the scope of this work to develop or apply a method to weight models such that the multi-model mean is statistically robust (Brunner et al., 2020).

2.3 Global warming level calculation

We calculated the global warming level following the methods of (Swaminathan et al., 2022). The global mean atmospheric surface temperature is calculated for each model, scenario and ensemble member. The anomaly is the difference from the mean of the period 1850-1900 from the relevant historical ensemble member. This temperature time series is then smoothed by taking the mean of a window with a width of 21 years, i.e. 10 years either side of the central year. The first year that the smoothed global mean surface temperature anomaly exceeds the global warming level is the GWL exceedance year (see Fig. 1 of (Swaminathan et al., 2022)). This work uses the 2°C, 3°C and 4°C GWLs, as described above.

We calculate the multi-model mean for each of the variables using the "one model - one vote" scheme described above. We also determine the multi-model mean GWLs and their timings from the multi-model mean temperature, instead of taking the weighted mean of the individual ensemble members GWLs timings. This method ensures that the multi-model mean is more representative of the overall ensemble, instead of biased towards only those models that reach the GWL.

We used the ESMValTool toolkit to perform the analysis. ESMValTool is a software toolkit that was built to facilitate the evaluation and inter-comparison of CMIP datasets by providing a set of modular and flexible tools (Righi et al., 2020). These tools include quick ways to standardise, slice, re-grid, and apply statistical operators to datasets. ESMValTool is hosted on

https://doi.org/10.5194/egusphere-2022-1483
Preprint. Discussion started: 4 January 2023

Table 1. A list of the models, the number of contributing ensemble members for each scenario, the model ECS, and the weighted mean ECS of the contributing models. The weighted ECS row shows how the model occupancy affects the mean ECS of the ensemble for each scenario. The presence or absence of models impacts the weighted ECS, but not the number of contributing ensemble members.

Model	Historical	SSP1-1.9	SSP1-2.6	SSP2-4.5	SSP3-7.0	SSP5-8.5	ECS, °C
ACCESS-ESM1-5	3		2	3	2	1	3.9
CESM2	3		3	3	3	3	5.15
CESM2-WACCM	3		1	3	1	3	4.68
CMCC-ESM2	1			1			3.57
CanESM5	10	10	10	10	10	10	5.64
CanESM5-CanOE	2		2	2	2		*5.64*
EC-Earth3-CC	8			8		1	4.1
IPSL-CM6A-LR	12	5	3	6	10	5	4.56
MIROC-ES2L	5	5	5	5	5	5	2.66
MPI-ESM1-2-LR	5	5	5	5	5	5	3.0
NorESM2-LM	2		1	2	1		2.56
UKESM1-0-LL	10	5	10	10	10	5	5.36
Total number of Ensembles	72	30	42	58	49	38	
Total number of Models	12	5	10	12	10	9	
Weighted ECS, °C	4.23	4.24	4.32	4.23	4.32	4.34	

GitHub and all the code we used here is available as described in the data availability section. This analysis was performed on the Centre for Environmental Data Analysis's (CEDA) JASMIN computing system. However, CMIP6 is so large that no data centre could host all datasets from all models. Absent datasets need to be copied from another ESGF node to the local system before they can be analysed.

3 Results

The total multi-model mean allocation of carbon for all available scenarios at each of the three warming levels is shown in fig. 2. There is a significant difference between both the total carbon in the system for different scenarios at the same warming level. For instance, the multi-model mean 2°C GWL ranges from 903 Pg in SSP5-8.5 to 948 Pg in SSP3-7.0. The carbon allocation between the three reservoirs for a given level varies between scenarios, even at the 2°C GWL. For instance, the multi-model mean 2°C GWL level land allocation fraction ranges from 29.6% to 32.6%, the ocean allocation ranges from 24.0% to 25.4% and the atmospheric fraction (AF) ranges from 42% to 46%. Similar variability ranges are present in the 3°C and 4°C GWL.

https://doi.org/10.5194/egusphere-2022-1483
Preprint. Discussion started: 4 January 2023

Experiments made with the highest CO_2 concentration scenario, SSP5-8.5, reach the warming thresholds with less total carbon in the Earth system, compared to other scenarios. For instance, 903 Pg in SSP5-8.5 to 933 Pg in SSP1-2.5. at 2°C GWL. Due to it's methane and aerosol precursor forcing, the SSP3-7.0 scenario is a special case, with behaviour quite different from the other scenarios, so these relationship may not hold for SSP3-7.0.

Similarly, the combined percentage of carbon allocated to the land surface and the ocean is smaller for the higher CO_2 concentration scenarios, ie the higher CO_2 concentration scenarios have a larger AF than lower CO_2 concentration scenarios at the same GWL. For instance, the AF is 46% in SSP5-8.5 and 42% SSP1-2.5 at the 2°C GWL, and the AF is 51.2% in SSP5-8.5 and 47.4% SSP2-4.5 at the 3°C GWL.

The total carbon in the atmosphere at any given point in time is the same for all models for a given scenario, but the multi-model mean shown here is an average over several different time periods for each scenario. For a given scenario, larger values of the total atmospheric carbon imply that the ensemble takes longer to reach the warming level. As a percentage, the anthropogenic carbon atmospheric fraction value reflects the relationship between the ensembles GWL timing and the ensembles mean ocean and land surface behaviour.

Not all scenarios are expected to reach all GWLs. While it's likely that all SSP5-8.5 will reach 2°C of warming, it is unlikely that any SSP1-1.9 experiments will reach 4°C of warming. On the other hand, in certain combinations of scenario and GWL, it's possible that only some models reach the threshold. For instance, some SSP1-1.9 models may reach the 2°C GWL and some may not. Figure 2 only shows the multi-model means, not single models. This means that multi-model means that do not reach the GWL are not included in this figure. For instance, the SSP1-1.9 multi-model mean does not reach 2°C of warming. This is known as survivor bias, with only the higher climate sensitivity models reaching the higher warming levels before the year 2100. As described above, the method that we used to populate this figure took the multi-model mean first with all models contributing equally, then used that value to calculate the GWL threshold years. An alternative method could first calculate the GWL threshold years for individual ensemble members, then take the mean of only those that reach the threshold. This alternative method would implicitly include survivor bias, causing the overall weighting to be biased towards high ECS models.

Table 1 shows that there are five models contributing to the SSP1-1.9 scenario in this analysis, yet the multi-model mean does not even reach the 2°GWL here. Similarly, there are 10 SSP1-2.6 models, but the multi-model mean does not reach the 3°(or 4°) GWL, and the mean of 12 SSP2-4.5 models does not reach the 4°of warming.

Figure 3 shows a breakdown of carbon allocation at each GWL as a percentage and the total value for each model. For each scenario and each GWL, the models are ordered by their ECS as shown in tab. 1. The lower ECS models are at the top and higher ECS models on the bottom of each section. The less sensitive models take longer to reach the same warming level and so generally have higher total emissions than the more sensitive models. This results in the saw-tooth pattern on the right of this figure. However, this saw-tooth is not visible on the left side of the figure, as the ratios of carbon allocation between land, ocean and atmosphere at a given GWL appear to be independent of ECS.

There is a significant difference in the carbon allocation structure at each GWL between scenarios in terms of the amount of total carbon. For instance, the lowest carbon allocation at 2°C is approximately 600 Pg, but the highest total carbon allocation is around 1500 Pg. When comparing between different GWLs, the highest total carbon allocation at the 2°C GWL (1500 Pg in

https://doi.org/10.5194/egusphere-2022-1483
Preprint. Discussion started: 4 January 2023

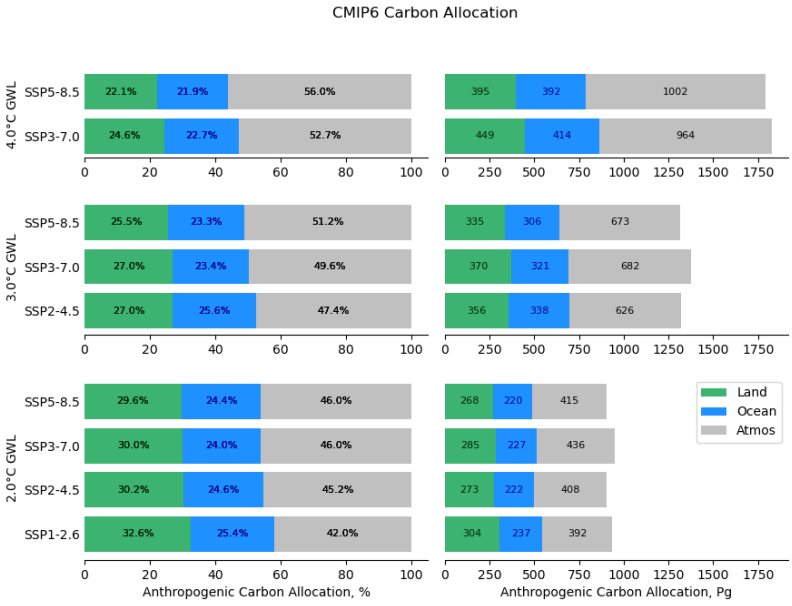

Figure 2. Carbon allocation for the multi-model mean for each scenario for each global warming level. The green, blue and grey areas represent the land, ocean and atmospheric carbon allocations. On the left hand side, the x-axis shows the carbon allocation as a percentage, and the right hand side shows the cumulative total.

NorESM2-LM SSP3-7.0) has more total carbon than several models at 4°C GWL, which can be as low as 1200 Pg. In essence, both CanESM5 models and the UKESM1 model reached 4°C of warming with less atmospheric carbon than NorESM2-LM had when it reached the 2°C of warming. This relates to the model's transient climate response to cumulative carbon emissions but highlights how badly constrained allowable carbon budgets can be. If these models were run in emission mode such that the carbon sinks could affect atmospheric CO_2 concentrations, the differences in carbon allocation may be even more significant. However, the opposite may also be possible; for instance if the land and ocean carbon sinks acted to change the atmospheric CO_2 concentrations in a way that would counteract the ECS effect of warming.

In contrast, the variability in the carbon allocation percentages is less obvious, but still important. For instance, the combined land and ocean allocation can be as low as 40% and as high as 60%. As was the case for the multi-model mean percentage allocation in fig.2, the higher CO_2 concentration scenarios have a smaller combined land and ocean carbon fraction than the lower CO_2 concentration scenarios for the same GWL. The SSP5-8.5 scenarios have a lower combined land and ocean carbon allocation than SSP1-1.9 and SSP1-2.6 scenarios, even at the same GWL. There is also variability between scenarios at the same warming level for a given model. One model, EC-Earth3-CC, has a particularly low land carbon allocation, approximately one third lower than the over ensemble mean. This makes it appear to be an outlier in this figure in the SSP2-4.5 and SSP5-8.5 scenarios where it contributes. This model has also had strange behaviour in other work Dunning et al. (2018).

https://doi.org/10.5194/egusphere-2022-1483
Preprint. Discussion started: 4 January 2023

As in fig. 2, survivor bias also affects this figure. For instance, the SSP1-1.9 scenario includes data from 5 models (see tab.1), yet only three models reach the 2°C GWL. Similarly, the SSP2-4.5 scenario includes data from 12 models (see tab.1), yet only two models reach the 4°C GWL. These missing models would probably reach the thresholds at some point after the year 2100, if the model were allowed to run for long enough and if the atmospheric carbon concentration were allowed to rise sufficiently high. In summary, fig. 3 shows that a model's sensitivity to CO_2 concentration significantly affects the total carbon allocation between the atmosphere, ocean and land at global warming levels, but is less impactful on the percentage allocation. In contrast, the scenario has a much larger impact on the percentage carbon allocation at a given warming level than the ECS.

The CMIP6 multi-model mean carbon allocation time series is shown in fig. 4. This figure includes a pair of panes for each experiment. For each pair, the top pane is the cumulative carbon in Pg and the bottom pane shows the percentage. The sum of the three sinks estimates the total anthropogenic emissions. The top left pair shows the development over the historical period and the other five are the future scenarios. We show all data cumulatively starting from the year 1850, and all the cumulative carbon panes share the same y-axis range. The times where each of the GWLs are reached are marked as vertical lines. The carbon allocation for the UKESM1 model is shown as dotted lines.

In the historical pane of fig. 4, the fractional atmospheric carbon starts to grow in the second half of the 20^{th} century, as the land fraction declines and the ocean fraction increases. However, all three increase in absolute terms over the historical period. By the end of the historical period, the land and ocean match the observational records of Raupach et al. (2014) and Watson et al. (2020) reasonably well, shown as dashed horizontal lines. In future scenarios, the global warming level threshold year occurs sooner in higher concentration scenarios than in lower concentrations scenarios. In all scenarios, the total anthropogenic carbon rises until at least the year 2050. The fraction of carbon that is absorbed by the combined land and ocean reservoirs rises in the two SSP1 scenarios, remains approximately constant in SSP2-4.5 after 2050, and declines in the SSP3-7.0 and SSP5-8.5 scenarios.

The combined land and ocean fraction rises in the SSP1-1.9 and SSP1-2.6 scenarios, this can be explained as the decline in emissions slowly percolating through the system and being absorbed by the ocean and land, without being replaced in the atmosphere by additional fossil fuel combustion. The time series results for the year 2100 closely match the IPCC AF forecast for 2100 (IPCC, 2021b, fig. SPM7), shown in fig. 4 as a horizontal line at the end of the period. This is not a new result, but allows increased confidence that our methods match previous results.

To see how carbon allocation varies between different scenarios in the absence of survivor bias and the irregular scenario contributions as shown in tab. 1, we can focus on a single model. We selected the UKESM1 model (labelled as UKESM1-0-LL in tab. 1 and fig. 3) as a focus. A full description of the UKESM1 model and it's CMIP6 representation are available in Sellar et al. (2019, 2020).

Figure 5 is similar to fig. 2, but for the mean of the single model UKESM1 ensemble. There is a much smoother transition between scenarios for each GWL, which reflects the fact that this group of measurements are free of the occupancy and survivor biases seen in fig. 2. For UKESM1, the difference between scenarios has an effect of several percent at a given GWL. The scenarios with higher CO_2 concentrations have a smaller combined ocean-land fraction of carbon allocation than those with low CO_2 concentrations. The land uptake almost always outweighs the ocean carbon allocation, with the exception of the

https://doi.org/10.5194/egusphere-2022-1483
Preprint. Discussion started: 4 January 2023

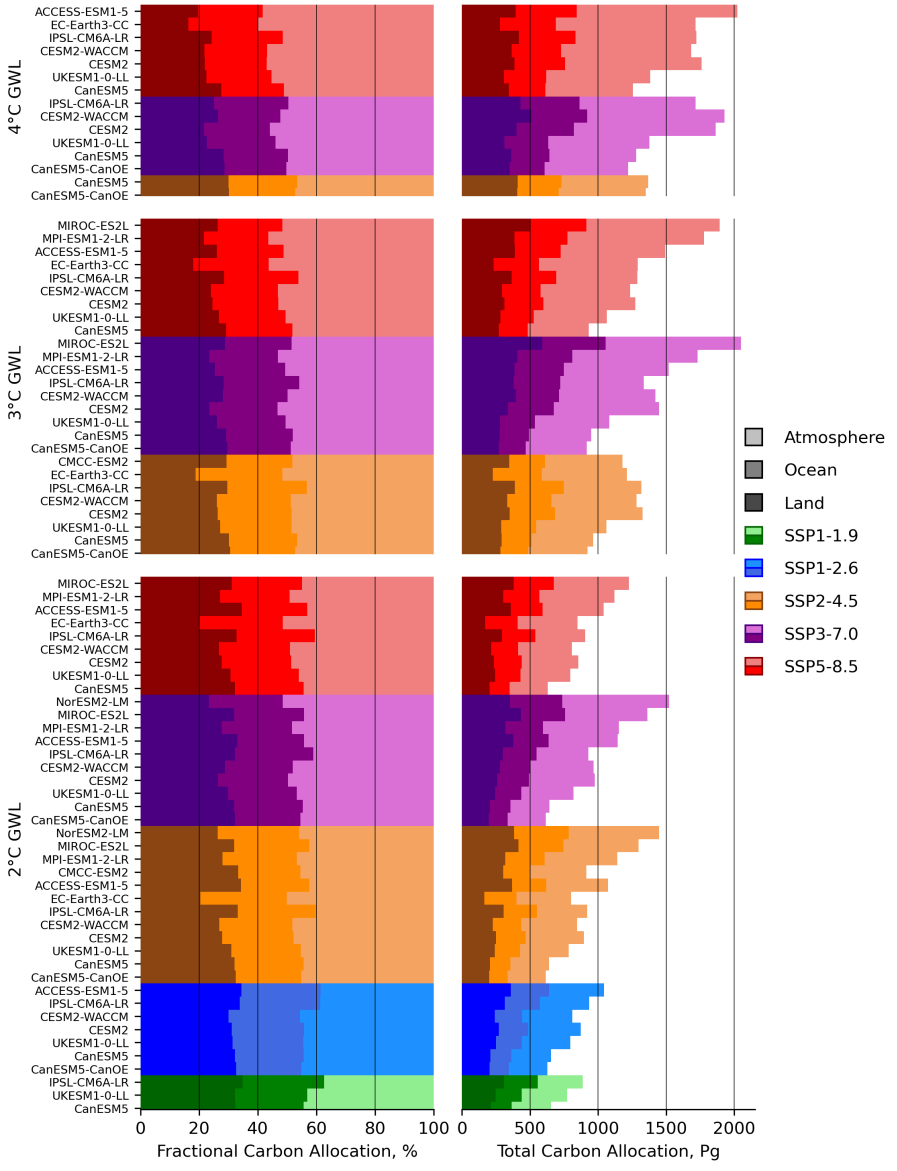

Figure 3. Global total carbon allocation for each level of warming for individual models. The left side shows the allocation as a percentage and the right side shows the total value in Pg. Each colour palette represents a different scenario, with SSP1-1.9 in greens, SSP1-2.6 in blues, SSP2-4.5 in golds, SSP3-7.0 in purples and SSP5-8.5 in reds. The darkest shade denotes the land, the middle shade is the ocean and the lightest shade is the atmosphere. Within a given GWL and scenario, the models are ordered by their ECS, with less sensitive models at the top and more sensitive models at the bottom.

SSP3-7.0 at 4°C of warming where the ocean uptakes 10 Pg more than the land. However, the land uptake has less variability between scenarios than the ocean at the same GWL. The range of uptakes between scenarios for the land range from 1 Pg (4°C

https://doi.org/10.5194/egusphere-2022-1483
Preprint. Discussion started: 4 January 2023

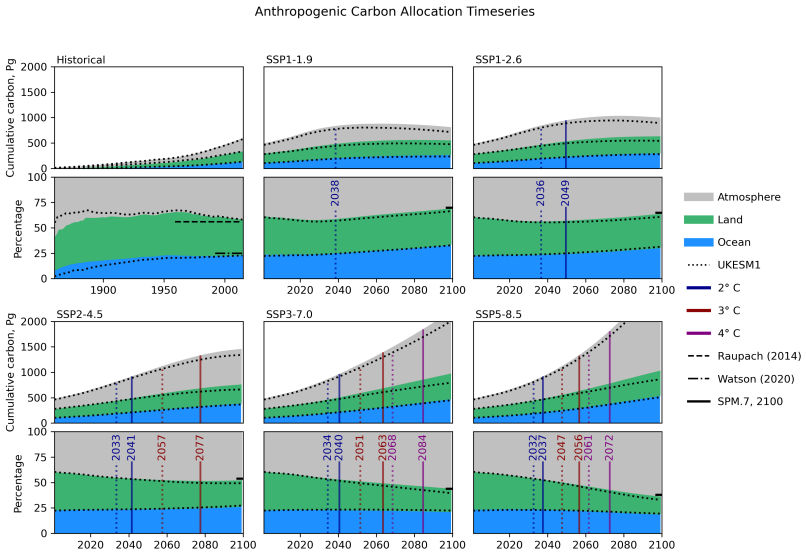

Figure 4. Multi-model mean carbon allocation time series for the historical period and each scenario. The top pane of each pair shows the total allocation in Pg, and the bottom pane shows the allocation as a percentage. The historical pane includes the historical observations from Raupach et al. (2014) & Watson et al. (2020), and the future pane shows the atmospheric fraction projection for 2100 from IPCC (2021b). The grey area is the cumulative anthropogenic carbon in the atmosphere, and the blue and green represent the fraction in the ocean and in the land, respectively. The UKESM1 model allocation is shown as dotted lines and it's GWL threshold years are shown as dotted vertical lines.

GWL) to 6 Pg (2°C GWL), where as the ocean ranges from 8 Pg (2°C GWL) to 16 Pg (3°C GWL). The variability in the ocean is likely due to the wider range of circulation behaviour in the scenarios. When compared to the multi-model mean in fig. 2, UKESM1 has a more significant relative ocean contribution and a smaller land contribution. This figure shows a decrease in the percentage of carbon taken up by the land as a function of GWL and hence as a function of total emitted CO_2. The higher CO_2 drives carbon uptake on land but this starts to saturate when growth is no longer CO_2 limited.

Figure 4 also shows the time series of carbon allocation for UKESM1. The most crucial difference between the UKESM1 and the multi-model mean is that the UKESM1 has an above average climate sensitivity to CO_2 so the GWL occur closer to the present day than in the multi-model mean. As was the case in the multi-model mean, the UKESM1's ocean fraction is more or less consistent throughout the SSP2-4.5, SSP3-7.0 and SSP5-8.5 scenarios, the land fraction declines from 35.2% at the end of the historical period to 22.0% in SSP2-4.5, 17.2% in SSP3-7.0 and 13.5% in SSP5-8.5 in the year 2100.

As for the multi-model ensemble, the UKESM1 reproduces the historical observations of Raupach et al. (2014) and Watson et al. (2020) in the recent past. However, UKESM1 tends to have a higher AF than the multi-model mean at the year 2100. In addition to hitting the GWL sooner, UKESM1's land and ocean components also absorb less total carbon than the multi-model mean at any given time. This means that the estimate of the total emissions is lower for UKESM1 than in the multi-model mean at the same point in time.

https://doi.org/10.5194/egusphere-2022-1483
Preprint. Discussion started: 4 January 2023

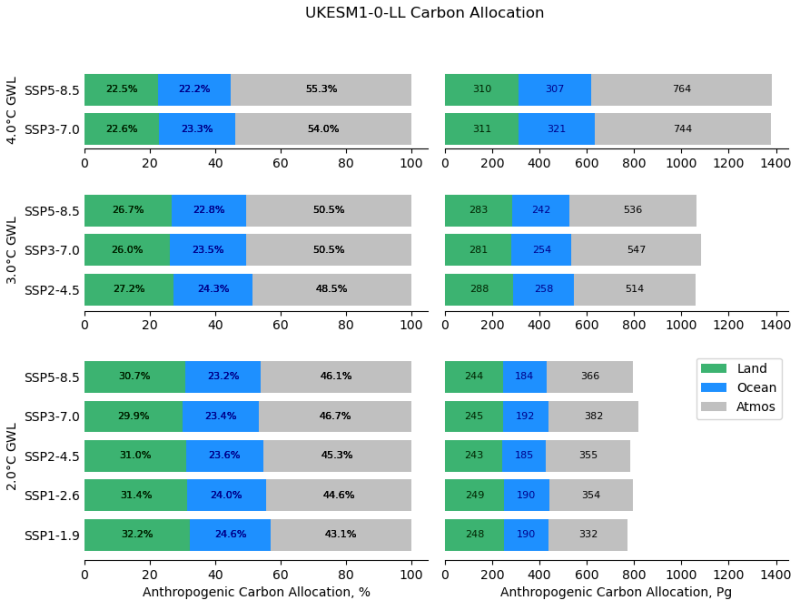

Figure 5. Global total carbon allocation for each level of warming for the UKESM1 model.

Together, figs. 4 and 5 show that for this model, the differences between scenario have a noticeable effect on carbon allocation. Fig. 4 shows a very strong sensitivity of the carbon allocation percentage in the land sink in terms of both scenario and GWL. The rate of decline in the land fraction is more negative in SSP5-8.5 than in SSP2-4.5. This might be because the warming is greater in SSP5-8.5 such that soil respiration, ocean stratification effects are proportionally stronger in the higher SSPs. Alternatively, with the more rapid increase in atmospheric CO_2, the land sink is unable to keep on absorbing atmospheric CO_2 and becomes limited in terms of photosynthetic uptake by Nitrogen limitation.

4 Discussion

The ensemble of CMIP6 models has a wide range of ECS values. The ECS primarily impacts how high the CO_2 concentration needs to be to reach a given GWL. A high ECS value means that GWL occur sooner and hence the concentration of CO_2 available to be absorbed by the land surface or the ocean is lower. For high ECS models to have a moderate TCRE, i.e. a moderate warming per unit of CO_2, the uptake of emitted CO_2 needs to be much more efficient than in low ECS models. A combination of high ECS and low carbon uptake efficiency (a high AF) leads to a very high TCRE. This is the case for the UKESM1 (Arora et al., 2020).

The choice of scenario impacts the ratio of carbon allocation in land, ocean and atmosphere for a given GWL. This means that even though two scenarios may reach the same warming level with similar atmospheric CO_2 concentrations, the ocean and the land surface absorb less carbon in the scenario with faster atmospheric CO_2 growth. As the atmospheric CO_2 concentration

https://doi.org/10.5194/egusphere-2022-1483
Preprint. Discussion started: 4 January 2023

directly influences warming rates, this reduction in the capacity of land surface and ocean to absorb CO_2 could lead to enhanced warming feedback in higher CO_2 concentrations scenarios, even with the same total emissions.

The scenario SSP3-7.0 often appears to be an outlier in these figures. For instance, in figs. 2 and 5, it does not conform to the pattern of the other scenarios. SSP3-7.0 is the scenario with the highest methane concentration and air pollution precursor emissions, even higher than SSP5-8.5 (Meinshausen et al., 2020). Methane is a strong greenhouse gas and has a warming effect (Meinshausen et al., 2017), but pollution precursor emissions are linked to aerosols and cloud formation, which generally have a cooling effect (Twomey, 1977). The balance of the warming methane emissions and the cooling aerosol precursors determines the impact on GWL. Therefore, SSP3-7.0 can reaches the GWLs earlier than other scenarios at the same CO_2 concentration, which is why the SSP3-7.0 has higher total carbon allocations than SSP5-8.5, notably in fig. 3. The impact of different methane and aerosol precursor emissions on the climate response is still in its infancy in terms of realism in CMIP6. The overall warming impact of methane is not considered in this work as is it secondary to CO_2 warming, but it could be examined in future extensions.

The difference between the minimum and maximum atmospheric fraction in the UKESM1 2°C GWL (43.1% in SSP1-1.9 and 46.7% SSP3-7.0,) is 3.6%. This may seem small, but it is equivalent to 50 Pg of additional carbon in the atmosphere. In the year 2020, 9.5±0.5 Pg of carbon was emitted globally (Friedlingstein et al., 2022), so this 3.6% difference alone is equivalent to around five years of our entire current total global emissions. Moving to a lower CO_2 concentrations scenario allows us to hit warming levels later, but also with less total carbon in the active carbon reservoirs.

The differences in carbon allocations seen here have consequences in the real world. Higher CO_2 suppresses global precipitation, as higher temperatures increase both global and regional precipitation changes (Tebaldi et al., 2021). As levels of CO_2 concentrations atmosphere increase, land ecosystems globally become progressively less efficient at absorbing carbon Wang et al. (2020). Higher CO_2 is causes enhanced ocean acidification, which has been shown to decrease survival, calcification, growth, development and abundance over a broad range of marine organisms (Kroeker et al., 2013).

In the highest CO_2 concentration scenarios, the land surface becomes saturated much sooner than the ocean. In these scenarios, the CO_2 concentration rises beyond the land surface's ability to maintain a constant absorption fraction. Meanwhile the ocean continues to keep the same allocation percentage and only shows a small decline in the highest CO_2 concentration scenarios.

The ocean fraction changes little in the high CO_2 concentration scenarios in the coming century, going from 24% at the end of the historical period to 27.1% in SSP2-4.5, 21.9% in SSP3-7.0, and 19.5% in SSP5-8.5 by the year 2100. A potential mechanistic explanation for the oceans behaviour would be that while the surface ocean might be CO_2 saturated, the rate at which surface waters and dissolved CO_2 is mixed downward will slow. This reduction is downward mixing reduces the overall absorption rate of CO_2 into the ocean. The increase in stratification is caused by warmer and more saline surface layers, combined with gradual decline in overturning rates and overall circulation (Thibodeau et al., 2018; Li et al., 2020; Caesar et al., 2021; Sallée et al., 2021). Ocean acidification may also be playing a role reducing the chemical transition of dissolved CO_2 and thus also slowing uptake Zeebe (2012). Combined together, these effects act to reduce the rate at which absorbed CO_2 is

https://doi.org/10.5194/egusphere-2022-1483
Preprint. Discussion started: 4 January 2023

removed from the surface layer. When the ocean fraction remains stationary, this means that the cumulative carbon absorbed by the ocean grows at a constant rate, proportionally to the estimate of the total emissions.

While the ocean fraction which is more or less consistent throughout the SSP2-4.5, SSP3-7.0 and SSP5-8.5 scenarios, the land fraction declines over the coming century, from 35.0% at the end of the historical period to 26.0% in SSP2-4.5, 23.1% in SSP3-7.0 and 17.9% in SSP5-8.5 in the year 2100. The land fraction is forecast to decline over the coming century in the higher CO_2 concentration scenarios, although the total land carbon allocation increases. There are several possible explanations for this slowdown of uptake. It might be that the soil respiration increases due to warming more than carbon uptake increase due to photosynthetic uptake (Nyberg and Hovenden, 2020) or that nitrogen limitation progressively limiting photosynthetic uptake (Ågren et al., 2012). Alternatively, the changing climate may impact vegetation growth and photosynthetic uptake via droughts and warming, which moves plants outside the most efficient temperatures for photosynthesis.

The UKESM1's higher AF at the year 2100 is likely due to the model limiting carbon uptake more than the other models. This could be Nitrogen limitation in the land surface or could be due to the models higher ECS and thus warmer temperatures at 2100 than the multi-model mean. The warmer temperatures impacts carbon uptake by having an increased soil respiration, a decreased ocean solubility of CO_2 and increased ocean stratification. All of which will decrease carbon uptake in UKESM1 relative to the multi-model mean. These processes may be correctly modelled in UKESM1 as a function of temperature and climate but their impact would be over-represented simply because there is more warming in UKESM1 than the multi-model mean due to the UKESM1s higher sensitivity.

In this work, we used concentration driven scenarios instead of emission driven scenarios. Emission driven scenarios allow significantly more flexibility in the behaviour of the atmospheric carbon, in effect adding a third degree of freedom into the calculation. Although a limited set of UKESM1 emission driven runs exist, it was found that there are actually very few differences in simulated temperature or atmospheric CO_2 concentration between concentration driven and emission driven scenarios (Lee et al., 2021, Sec. 4.3.1.1). In any case, several key datasets required in the calculation of the LUE in eq. 1 were not available in the emissions driven experiments at the time of writing.

While we made every effort to build a uniform ensemble, ScenarioMIP's flexible contributions means that we have a non-trivial diversity in data occupancy between scenarios. The SSP5-8.5 ensemble has the highest mean ECS, meaning that the multi-model mean of this ensemble will likely be warmer than other scenarios multi-model mean's at the same atmospheric carbon concentration. While this is a small effect here, future versions of this study will likely need to take this into account. Similarly, we were fortunate that the mean ECS of our SSP1-1.9 ensemble falls in a similar range to the other scenarios. Our conclusions may have been different if more models had provided SSP1-1.9 simulations. This is one of the key results of this analysis: any result looking at the behaviour of the multi-model mean needs to be careful with handling the equilibrium climate sensitivity bias of the ensemble. Two multi-model means of different scenarios may not always be directly comparable.

https://doi.org/10.5194/egusphere-2022-1483
Preprint. Discussion started: 4 January 2023

5 Conclusions

Using an ensemble of CMIP6 simulations, we have shown that the carbon allocation between Earth System components varies significantly with the scenario pathway. Scenarios with higher carbon concentrations reach the global warming levels sooner, and have proportionally less carbon allocated to the ocean and land surface at that time. The differences in estimated carbon emissions between scenarios vary even at the same GWL, and can be equivalent to several years worth of global total emissions.

At two degrees C of warming, the atmospheric fraction ranges from 42% to 46%, the ocean fraction ranges from 24% to to 25.6%, and the land fraction ranges from 29.6% to 32.6%. At four degrees of warming, the atmospheric fraction ranges from 54.0% to 55.3%, the ocean fraction ranges from 22.2% to to 23.3%, and the land fraction ranges from 22.5% to 22.6%. Meanwhile, the historical observations have an atmospheric fraction of 56% (Raupach et al., 2014) an ocean fraction of 25% and a land fraction of 19% (Watson et al., 2020). Scenarios with higher integrated emissions (e.g. SSP3-7.0 and SSP5-8.5) typically reach GWLs sooner, with higher atmospheric CO_2 concentrations, and greater fractions of emitted CO_2 remaining in the atmosphere and driving climate warming. In the lower emission scenarios, the atmospheric fraction declines, the land fraction remains constant and the ocean fraction rises. In contrast, lower integrated emissions scenarios (e.g. SSP1-1.9, SSP1-2.6 and SSP2-4.5) can reach the same GWLs, but they do so more slowly, with greater fractions of emitted CO_2 absorbed from the atmosphere into ocean and land components, reducing and slowing overall climate warming.

A model's sensitivity to CO_2 concentration significantly affects the total carbon allocation between the atmosphere, ocean and land at all global warming levels. In contrast, the choice of scenario has a much larger impact on the percentage carbon allocation at a given warming level than a model's ECS.

Ultimately, across all model simulations, a significant rise in global mean surface temperature is projected over the 21^{st} century. This underscores the need for an accelerating transition to low carbon technologies to reduce the risk of the worst effects of climate change.

Code and data availability. This analysis was performed using ESMValTool, and the software tools are available via both github for an up to date version of the base system and via zenodo for the specific branch that was used to generate this analysis. CMIP6 climate model data used in this paper was obtained from the CEDA's Earth System Federation Grid node, and is widely available.

Author contributions. All authors contributed to the writing, discussion, initial outline, literature survey and editorial feedback of the manuscript. LdM led the work, performed the analyses, led the writing. RS, CGJ, LDM developed the GWL analysis methods. CDJ, SL, TQ contributed to the land surface carbon calculation. JW contributed to the extraction and curation of the model data. CGJ, JB, led the UKESM1 and TerraFimra project working groups where this work was funded.

Competing interests. The authors are not aware of any competing interests.

https://doi.org/10.5194/egusphere-2022-1483
Preprint. Discussion started: 4 January 2023

Acknowledgements. LdM and DIK were supported by the UK Natural Environment Research Council through The UK Earth System Modelling Project (UKESM, grant no. NE/N017951/1). RS, RJP, TQ and RPA are funded by the UK National Centre for Earth Observation (NE/N018079/1). LdM, RS, RJP, CDJ, CGJ, AY were supported by the UK Natural Environment Research Council through the TerraFIRMA: Future Impacts, Risks and Mitigation Actions in a changing Earth system project, Grant reference NE/W004895/1. CGJ acknowledges funding from the NERC National Capability UKESM grant no. NE/N017978/1 and EU Horizon 2020 project CRESCENDO, grant number: 641816. CDJ, SL and JW were supported by the Joint UK BEIS/Defra Met Office Hadley Centre Climate Programme (GA01101) CDJ was supported by the European Union's Horizon 2020 research and innovation programme under Grant Agreement No 101003536 (ESM2025 - Earth System Models for the Future). The authors would also like to thank the JASMIN and ESMValTool teams for their assistance with this work.

https://doi.org/10.5194/egusphere-2022-1483
Preprint. Discussion started: 4 January 2023

References

Arias, P., Bellouin, N., Coppola, E., Jones, R., Krinner, G., Marotzke, J., Naik, V., Palmer, M., Plattner, G.-K., Rogelj, J., Rojas, M., Sillmann, J., Storelvmo, T., Thorne, P., Trewin, B., Achuta Rao, K., Adhikary, B., Allan, R., Armour, K., Bala, G., Barimalala, R., Berger, S., Canadell, J., Cassou, C., Cherchi, A., Collins, W., Collins, W., Connors, S., Corti, S., Cruz, F., Dentener, F., Dereczynski, C., Di Luca, A., Diongue Niang, A., Doblas-Reyes, F., Dosio, A., Douville, H., Engelbrecht, F., Eyring, V., Fischer, E., Forster, P., Fox-Kemper, B., Fuglestvedt, J., Fyfe, J., Gillett, N., Goldfarb, L., Gorodetskaya, I., Gutierrez, J., Hamdi, R., Hawkins, E., Hewitt, H., Hope, P., Islam, A., Jones, C., Kaufman, D., Kopp, R., Kosaka, Y., Kossin, J., Krakovska, S., Lee, J.-Y., Li, J., Mauritsen, T., Maycock, T., Meinshausen, M., Min, S.-K., Monteiro, P., Ngo-Duc, T., Otto, F., Pinto, I., Pirani, A., Raghavan, K., Ranasinghe, R., Ruane, A., Ruiz, L., Sallée, J.-B., Samset, B., Sathyendranath, S., Seneviratne, S., Sörensson, A., Szopa, S., Takayabu, I., Tréguier, A.-M., van den Hurk, B., Vautard, R., von Schuckmann, K., Zaehle, S., Zhang, X., and Zickfeld, K.: Technical Summary, p. 33-144, Cambridge University Press, Cambridge, United Kingdom and New York, NY, USA, https://doi.org/10.1017/9781009157896.002, 2021.

Arora, V. K., Katavouta, A., Williams, R. G., Jones, C. D., Brovkin, V., Friedlingstein, P., Schwinger, J., Bopp, L., Boucher, O., Cadule, P., Chamberlain, M. A., Christian, J. R., Delire, C., Fisher, R. A., Hajima, T., Ilyina, T., Joetzjer, E., Kawamiya, M., Koven, C. D., Krasting, J. P., Law, R. M., Lawrence, D. M., Lenton, A., Lindsay, K., Pongratz, J., Raddatz, T., Séférian, R., Tachiiri, K., Tjiputra, J. F., Wiltshire, A., Wu, T., and Ziehn, T.: Carbon–concentration and carbon–climate feedbacks in CMIP6 models and their comparison to CMIP5 models, Biogeosciences, 17, 4173–4222, https://doi.org/10.5194/bg-17-4173-2020, 2020.

Brunner, L., Pendergrass, A. G., Lehner, F., Merrifield, A. L., Lorenz, R., and Knutti, R.: Reduced global warming from CMIP6 projections when weighting models by performance and independence, Earth System Dynamics, 11, 995–1012, https://doi.org/10.5194/esd-11-995-2020, 2020.

Burton, C., Kelley, D. I., Jones, C. D., Betts, R. A., Cardoso, M., and Anderson, L.: South American fires and their impacts on ecosystems increase with continued emissions, Climate Resilience and Sustainability, 1, e8, https://doi.org/https://doi.org/10.1002/cli2.8, 2022.

Caesar, L., McCarthy, G. D., Thornalley, D. J. R., Cahill, N., and Rahmstorf, S.: Current Atlantic Meridional Overturning Circulation weakest in last millennium, Nature Geoscience, 14, 118–120, https://doi.org/10.1038/s41561-021-00699-z, 2021.

Caldeira, K. and Wickett, M. E.: Anthropogenic carbon and ocean pH, Nature, 425, 365–365, https://doi.org/10.1038/425365a, 2003.

Collection, U. N. T.: Paris Agreement, https://treaties.un.org/pages/ViewDetails.aspx?src=TREATY&mtdsg_no=XXVII-7-d&chapter=27&clang=_en, 2015.

Dunning, C. M., Black, E., and Allan, R. P.: Later Wet Seasons with More Intense Rainfall over Africa under Future Climate Change, Journal of Climate, 31, 9719 – 9738, https://doi.org/10.1175/JCLI-D-18-0102.1, 2018.

Erda, L., Wei, X., Hui, J., Yinlong, X., Yue, L., Liping, B., and Liyong, X.: Climate change impacts on crop yield and quality with CO2 fertilization in China., Philos Trans R Soc Lond B Biol Sci., 360, 2149 – 2154, https://doi.org/doi/10.1098/rstb.2005.1743, 2005.

Eyring, V., Bony, S., Meehl, G. A., Senior, C. A., Stevens, B., Stouffer, R. J., and Taylor, K. E.: Overview of the Coupled Model Intercomparison Project Phase 6 (CMIP6) experimental design and organization, Geoscientific Model Development, 9, 1937–1958, https://doi.org/10.5194/gmd-9-1937-2016, 2016.

Friedlingstein, P., Jones, M. W., O'Sullivan, M., Andrew, R. M., Bakker, D. C. E., Hauck, J., Le Quéré, C., Peters, G. P., Peters, W., Pongratz, J., Sitch, S., Canadell, J. G., Ciais, P., Jackson, R. B., Alin, S. R., Anthoni, P., Bates, N. R., Becker, M., Bellouin, N., Bopp, L., Chau, T. T. T., Chevallier, F., Chini, L. P., Cronin, M., Currie, K. I., Decharme, B., Djeutchouang, L. M., Dou, X., Evans, W., Feely, R. A., Feng, L., Gasser, T., Gilfillan, D., Gkritzalis, T., Grassi, G., Gregor, L., Gruber, N., Gürses, O., Harris, I., Houghton, R. A., Hurtt, G. C., Iida,

https://doi.org/10.5194/egusphere-2022-1483
Preprint. Discussion started: 4 January 2023

Y., Ilyina, T., Luijkx, I. T., Jain, A., Jones, S. D., Kato, E., Kennedy, D., Klein Goldewijk, K., Knauer, J., Korsbakken, J. I., Körtzinger, A., Landschützer, P., Lauvset, S. K., Lefèvre, N., Lienert, S., Liu, J., Marland, G., McGuire, P. C., Melton, J. R., Munro, D. R., Nabel, J. E. M. S., Nakaoka, S.-I., Niwa, Y., Ono, T., Pierrot, D., Poulter, B., Rehder, G., Resplandy, L., Robertson, E., Rödenbeck, C., Rosan, T. M., Schwinger, J., Schwingshackl, C., Séférian, R., Sutton, A. J., Sweeney, C., Tanhua, T., Tans, P. P., Tian, H., Tilbrook, B., Tubiello, F., van der Werf, G. R., Vuichard, N., Wada, C., Wanninkhof, R., Watson, A. J., Willis, D., Wiltshire, A. J., Yuan, W., Yue, C., Yue, X., Zaehle, S., and Zeng, J.: Global Carbon Budget 2021, Earth System Science Data, 14, 1917–2005, https://doi.org/10.5194/essd-14-1917-2022, 2022.

Gregory, J. M., Ingram, W. J., Palmer, M. A., Jones, G. S., Stott, P. A., Thorpe, R. B., Lowe, J. A., Johns, T. C., and Williams, K. D.: A new method for diagnosing radiative forcing and climate sensitivity, Geophysical Research Letters, 31, https://doi.org/https://doi.org/10.1029/2003GL018747, 2004.

Hansen, J., Johnson, D., Lacis, A., Lebedeff, S., Lee, P., Rind, D., and Russell, G.: Climate Impact of Increasing Atmospheric Carbon Dioxide, Science, 213, 957–966, https://doi.org/10.1126/science.213.4511.957, 1981.

Hauck, J., Zeising, M., Le Quéré, C., Gruber, N., Bakker, D. C. E., Bopp, L., Chau, T. T. T., G urses, O., Ilyina, T., Landschützer, P., Lenton, A., Resplandy, L., Rödenbeck, C., Schwinger, J., and Séférian, R.: Consistency and Challenges in the Ocean Carbon Sink Estimate for the Global Carbon Budget, Frontiers in Marine Science, 7, https://doi.org/10.3389/fmars.2020.571720, 2020.

Hausfather, Z.: https://www.carbonbrief.org/cmip6-the-next-generation-of-climate-models-explained/, accessed: 2022-12-21, 2022.

IPCC: Climate Change 2021: The Physical Science Basis. Contribution of Working Group I to the Sixth Assessment Report of the Intergovernmental Panel on Climate Change, vol. In Press, Cambridge University Press, Cambridge, United Kingdom and New York, NY, USA, https://doi.org/10.1017/9781009157896, 2021a.

IPCC: Summary for Policymakers, p. 3-32, Cambridge University Press, Cambridge, United Kingdom and New York, NY, USA, https://doi.org/10.1017/9781009157896.001, 2021b.

Jacobson, A. R., Mikaloff Fletcher, S. E., Gruber, N., Sarmiento, J. L., and Gloor, M.: A joint atmosphere-ocean inversion for surface fluxes of carbon dioxide: 2. Regional results, Global Biogeochemical Cycles, 21, https://doi.org/https://doi.org/10.1029/2006GB002703, 2007.

Jones, C., Robertson, E., Arora, V., Friedlingstein, P., Shevliakova, E., Bopp, L., Brovkin, V., Hajima, T., Kato, E., Kawamiya, M., Liddicoat, S., Lindsay, K., Reick, C. H., Roelandt, C., Segschneider, J., and Tjiputra, J.: Twenty-First-Century Compatible CO2 Emissions and Airborne Fraction Simulated by CMIP5 Earth System Models under Four Representative Concentration Pathways, Journal of Climate, 26, 4398 – 4413, https://doi.org/10.1175/JCLI-D-12-00554.1, 2013.

Jones, C. D., Hughes, J. K., Bellouin, N., Hardiman, S. C., Jones, G. S., Knight, J., Liddicoat, S., O'Connor, F. M., Andres, R. J., Bell, C., Boo, K.-O., Bozzo, A., Butchart, N., Cadule, P., Corbin, K. D., Doutriaux-Boucher, M., Friedlingstein, P., Gornall, J., Gray, L., Halloran, P. R., Hurtt, G., Ingram, W. J., Lamarque, J.-F., Law, R. M., Meinshausen, M., Osprey, S., Palin, E. J., Parsons Chini, L., Raddatz, T., Sanderson, M. G., Sellar, A. A., Schurer, A., Valdes, P., Wood, N., Woodward, S., Yoshioka, M., and Zerroukat, M.: The HadGEM2-ES implementation of CMIP5 centennial simulations, Geoscientific Model Development, 4, 543–570, https://doi.org/10.5194/gmd-4-543-2011, 2011.

Jones, C. D., Arora, V., Friedlingstein, P., Bopp, L., Brovkin, V., Dunne, J., Graven, H., Hoffman, F., Ilyina, T., John, J. G., Jung, M., Kawamiya, M., Koven, C., Pongratz, J., Raddatz, T., Randerson, J. T., and Zaehle, S.: C4MIP – The Coupled Climate–Carbon Cycle Model Intercomparison Project: experimental protocol for CMIP6, Geoscientific Model Development, 9, 2853–2880, https://doi.org/10.5194/gmd-9-2853-2016, 2016.

https://doi.org/10.5194/egusphere-2022-1483
Preprint. Discussion started: 4 January 2023

Kroeker, K. J., Kordas, R. L., Crim, R., Hendriks, I. E., Ramajo, L., Singh, G. S., Duarte, C. M., and Gattuso, J.-P.: Impacts of ocean acidification on marine organisms: quantifying sensitivities and interaction with warming, Global Change Biology, 19, 1884–1896, https://doi.org/https://doi.org/10.1111/gcb.12179, 2013.

Lee, J.-Y., Marotzke, J., Bala, G., Cao, L., Corti, S., Dunne, J., Engelbrecht, F., Fischer, E., Fyfe, J., Jones, C., Maycock, A., Mutemi, J., Ndiaye, O., Panickal, S., and Zhou, T.: Future Global Climate: Scenario-Based Projections and Near-Term Information, p. 553–672, Cambridge University Press, Cambridge, United Kingdom and New York, NY, USA, https://doi.org/10.1017/9781009157896.006, 2021.

Li, G., Cheng, L., Zhu, J., Trenberth, K. E., Mann, M. E., and Abraham, J. P.: Increasing ocean stratification over the past half-century, Nature Climate Change, 10, 1116–1123, https://doi.org/10.1038/s41558-020-00918-2, 2020.

Liddicoat, S. K., Wiltshire, A. J., Jones, C. D., Arora, V. K., Brovkin, V., Cadule, P., Hajima, T., Lawrence, D. M., Pongratz, J., Schwinger, J., Séférian, R., Tjiputra, J. F., and Ziehn, T.: Compatible Fossil Fuel CO2 Emissions in the CMIP6 Earth System Models' Historical and Shared Socioeconomic Pathway Experiments of the Twenty-First Century, Journal of Climate, 34, 2853 – 2875, https://doi.org/10.1175/JCLI-D-19-0991.1, 2021.

Lovato, T., Peano, D., Butenschön, M., Materia, S., Iovino, D., Scoccimarro, E., Fogli, P. G., Cherchi, A., Bellucci, A., Gualdi, S., Masina, S., and Navarra, A.: CMIP6 Simulations With the CMCC Earth System Model (CMCC-ESM2), Journal of Advances in Modeling Earth Systems, 14, e2021MS002 814, https://doi.org/https://doi.org/10.1029/2021MS002814, e2021MS002814 2021MS002814, 2022.

Meinshausen, M., Vogel, E., Nauels, A., Lorbacher, K., Meinshausen, N., Etheridge, D. M., Fraser, P. J., Montzka, S. A., Rayner, P. J., Trudinger, C. M., Krummel, P. B., Beyerle, U., Canadell, J. G., Daniel, J. S., Enting, I. G., Law, R. M., Lunder, C. R., O'Doherty, S., Prinn, R. G., Reimann, S., Rubino, M., Velders, G. J. M., Vollmer, M. K., Wang, R. H. J., and Weiss, R.: Historical greenhouse gas concentrations for climate modelling (CMIP6), Geoscientific Model Development, 10, 2057–2116, https://doi.org/10.5194/gmd-10-2057-2017, 2017.

Meinshausen, M., Nicholls, Z. R. J., Lewis, J., Gidden, M. J., Vogel, E., Freund, M., Beyerle, U., Gessner, C., Nauels, A., Bauer, N., Canadell, J. G., Daniel, J. S., John, A., Krummel, P. B., Luderer, G., Meinshausen, N., Montzka, S. A., Rayner, P. J., Reimann, S., Smith, S. J., van den Berg, M., Velders, G. J. M., Vollmer, M. K., and Wang, R. H. J.: The shared socio-economic pathway (SSP) greenhouse gas concentrations and their extensions to 2500, Geoscientific Model Development, 13, 3571–3605, https://doi.org/10.5194/gmd-13-3571-2020, 2020.

Myers, N.: Carbon Dioxide Review, Environmental Conservation, 10, 370–371, https://doi.org/10.1017/S0376892900013345, 1983.

Nyberg, M. and Hovenden, M. J.: Warming increases soil respiration in a carbon-rich soil without changing microbial respiratory potential, Biogeosciences, 17, 4405–4420, https://doi.org/10.5194/bg-17-4405-2020, 2020.

O'Neill, B. C., Tebaldi, C., van Vuuren, D. P., Eyring, V., Friedlingstein, P., Hurtt, G., Knutti, R., Kriegler, E., Lamarque, J.-F., Lowe, J., Meehl, G. A., Moss, R., Riahi, K., and Sanderson, B. M.: The Scenario Model Intercomparison Project (ScenarioMIP) for CMIP6, Geoscientific Model Development, 9, 3461–3482, https://doi.org/10.5194/gmd-9-3461-2016, 2016.

Raupach, M. R., Gloor, M., Sarmiento, J. L., Canadell, J. G., Frölicher, T. L., Gasser, T., Houghton, R. A., Le Quéré, C., and Trudinger, C. M.: The declining uptake rate of atmospheric CO_2 by land and ocean sinks, Biogeosciences, 11, 3453–3475, https://doi.org/10.5194/bg-11-3453-2014, 2014.

Resplandy, L., Keeling, R., Rödenbeck, C., Stephens, B. B., Khatiwala, S., Rodgers, K., Long, M. C., Bopp, L., and Tans, P. P.: Revision of global carbon fluxes based on a reassessment of oceanic and riverine carbon transport, Nature Geoscience, 11, 504—509, https://doi.org/10.1038/s41561-018-0151-3, 2018.

Riahi, K., van Vuuren, D. P., Kriegler, E., Edmonds, J., O'Neill, B. C., Fujimori, S., Bauer, N., Calvin, K., Dellink, R., Fricko, O., Lutz, W., Popp, A., Cuaresma, J. C., KC, S., Leimbach, M., Jiang, L., Kram, T., Rao, S., Emmerling, J., Ebi, K., Hasegawa, T.,

https://doi.org/10.5194/egusphere-2022-1483
Preprint. Discussion started: 4 January 2023

Havlik, P., Humpenöder, F., Da Silva, L. A., Smith, S., Stehfest, E., Bosetti, V., Eom, J., Gernaat, D., Masui, T., Rogelj, J., Strefler, J., Drouet, L., Krey, V., Luderer, G., Harmsen, M., Takahashi, K., Baumstark, L., Doelman, J. C., Kainuma, M., Klimont, Z., Marangoni, G., Lotze-Campen, H., Obersteiner, M., Tabeau, A., and Tavoni, M.: The Shared Socioeconomic Pathways and their energy, land use, and greenhouse gas emissions implications: An overview, Global Environmental Change, 42, 153–168, https://doi.org/https://doi.org/10.1016/j.gloenvcha.2016.05.009, 2017.

Righi, M., Andela, B., Eyring, V., Lauer, A., Predoi, V., Schlund, M., Vegas-Regidor, J., Bock, L., Brötz, B., de Mora, L., Diblen, F., Dreyer, L., Drost, N., Earnshaw, P., Hassler, B., Koldunov, N., Little, B., Loosveldt Tomas, S., and Zimmermann, K.: Earth System Model Evaluation Tool (ESMValTool) v2.0 – technical overview, Geoscientific Model Development, 13, 1179–1199, https://doi.org/10.5194/gmd-13-1179-2020, 2020.

Roser, M. and Ritchie, H.: Oil Spills, Our World in Data, https://ourworldindata.org/oil-spills, 2022.

Sallée, J.-B., Pellichero, V., Akhoudas, C., Pauthenet, E., Vignes, L., Schmidtko, S., Garabato, A. N., Sutherland, P., and Kuusela, M.: Summertime increases in upper-ocean stratification and mixed-layer depth, Nature, 591, 592–598, https://doi.org/10.1038/s41586-021-03303-x, 2021.

Schlunegger, S., Rodgers, K. B., Sarmiento, J. L., Frölicher, T. L., Dunne, J. P., Ishii, M., and Slater, R.: Emergence of anthropogenic signals in the ocean carbon cycle, Nature Climate Change, 9, 719–725, https://doi.org/10.1038/s41558-019-0553-2, 2019.

Sellar, A. A., Jones, C. G., Mulcahy, J. P., Tang, Y., Yool, A., Wiltshire, A., O'Connor, F. M., Stringer, M., Hill, R., Palmieri, J., Woodward, S., de Mora, L., Kuhlbrodt, T., Rumbold, S. T., Kelley, D. I., Ellis, R., Johnson, C. E., Walton, J., Abraham, N. L., Andrews, M. B., Andrews, T., Archibald, A. T., Berthou, S., Burke, E., Blockley, E., Carslaw, K., Dalvi, M., Edwards, J., Folberth, G. A., Gedney, N., Griffiths, P. T., Harper, A. B., Hendry, M. A., Hewitt, A. J., Johnson, B., Jones, A., Jones, C. D., Keeble, J., Liddicoat, S., Morgenstern, O., Parker, R. J., Predoi, V., Robertson, E., Siahaan, A., Smith, R. S., Swaminathan, R., Woodhouse, M. T., Zeng, G., and Zerroukat, M.: UKESM1: Description and Evaluation of the U.K. Earth System Model, Journal of Advances in Modeling Earth Systems, 11, 4513–4558, https://doi.org/https://doi.org/10.1029/2019MS001739, 2019.

Sellar, A. A., Walton, J., Jones, C. G., Wood, R., Abraham, N. L., Andrejczuk, M., Andrews, M. B., Andrews, T., Archibald, A. T., de Mora, L., Dyson, H., Elkington, M., Ellis, R., Florek, P., Good, P., Gohar, L., Haddad, S., Hardiman, S. C., Hogan, E., Iwi, A., Jones, C. D., Johnson, B., Kelley, D. I., Kettleborough, J., Knight, J. R., Köhler, M. O., Kuhlbrodt, T., Liddicoat, S., Linova-Pavlova, I., Mizielinski, M. S., Morgenstern, O., Mulcahy, J., Neininger, E., O'Connor, F. M., Petrie, R., Ridley, J., Rioual, J.-C., Roberts, M., Robertson, E., Rumbold, S., Seddon, J., Shepherd, H., Shim, S., Stephens, A., Teixiera, J. C., Tang, Y., Williams, J., Wiltshire, A., and Griffiths, P. T.: Implementation of U.K. Earth System Models for CMIP6, Journal of Advances in Modeling Earth Systems, 12, e2019MS001 946, https://doi.org/https://doi.org/10.1029/2019MS001946, e2019MS001946 10.1029/2019MS001946, 2020.

Sherwood, S. C., Webb, M. J., Annan, J. D., Armour, K. C., Forster, P. M., Hargreaves, J. C., Hegerl, G., Klein, S. A., Marvel, K. D., Rohling, E. J., Watanabe, M., Andrews, T., Braconnot, P., Bretherton, C. S., Foster, G. L., Hausfather, Z., von der Heydt, A. S., Knutti, R., Mauritsen, T., Norris, J. R., Proistosescu, C., Rugenstein, M., Schmidt, G. A., Tokarska, K. B., and Zelinka, M. D.: An Assessment of Earth's Climate Sensitivity Using Multiple Lines of Evidence, Reviews of Geophysics, 58, e2019RG000 678, https://doi.org/https://doi.org/10.1029/2019RG000678, e2019RG000678 2019RG000678, 2020.

Sullivan, A., Baker, E., and Kurvits, T.: Spreading Like Wildfire: The Rising Threat of Extraordinary Landscape Fires, Tech. rep., UN Environment Program, https://policycommons.net/artifacts/2259313/wildfire_rra/, 2022.

https://doi.org/10.5194/egusphere-2022-1483
Preprint. Discussion started: 4 January 2023

Swaminathan, R., Parker, R. J., Jones, C. G., Allan, R. P., Quaife, T., Kelley, D. I., de Mora, L., and Walton, J.: The Physical Climate at Global Warming Thresholds as Seen in the U.K. Earth System Model, Journal of Climate, 35, 29 – 48, https://doi.org/10.1175/JCLI-D-21-0234.1, 2022.

Tebaldi, C., Debeire, K., Eyring, V., Fischer, E., Fyfe, J., Friedlingstein, P., Knutti, R., Lowe, J., O'Neill, B., Sanderson, B., van Vuuren, D., Riahi, K., Meinshausen, M., Nicholls, Z., Tokarska, K. B., Hurtt, G., Kriegler, E., Lamarque, J.-F., Meehl, G., Moss, R., Bauer, S. E., Boucher, O., Brovkin, V., Byun, Y.-H., Dix, M., Gualdi, S., Guo, H., John, J. G., Kharin, S., Kim, Y., Koshiro, T., Ma, L., Olivié, D., Panickal, S., Qiao, F., Rong, X., Rosenbloom, N., Schupfner, M., Séférian, R., Sellar, A., Semmler, T., Shi, X., Song, Z., Steger, C., Stouffer, R., Swart, N., Tachiiri, K., Tang, Q., Tatebe, H., Voldoire, A., Volodin, E., Wyser, K., Xin, X., Yang, S., Yu, Y., and Ziehn, T.: Climate model projections from the Scenario Model Intercomparison Project (ScenarioMIP) of CMIP6, Earth System Dynamics, 12, 253–293, https://doi.org/10.5194/esd-12-253-2021, 2021.

Thibodeau, B., Not, C., Zhu, J., Schmittner, A., Noone, D., Tabor, C., Zhang, J., and Liu, Z.: Last Century Warming Over the Canadian Atlantic Shelves Linked to Weak Atlantic Meridional Overturning Circulation, Geophysical Research Letters, 45, 12,376–12,385, https://doi.org/https://doi.org/10.1029/2018GL080083, 2018.

Twomey, S.: The Influence of Pollution on the Shortwave Albedo of Clouds, Journal of Atmospheric Sciences, 34, 1149 – 1152, https://doi.org/10.1175/1520-0469(1977)034<1149:TIOPOT>2.0.CO;2, 1977.

Ukkola, A. M., Prentice, I., Keenan, T. F., van Dijk, A. I., Viney, N. R., Myneni, R., and Bi, J.: Reduced streamflow in water-stressed climates consistent with CO2 effects on vegetation, Nature Climate Change, 6, 75–78, https://doi.org/10.1038/nclimate2831, 2016.

Wang, S., Zhang, Y., Ju, W., Chen, J. M., Ciais, P., Cescatti, A., Sardans, J., Janssens, I. A., Wu, M., Berry, J. A., Campbell, E., Fernández-Martínez, M., Alkama, R., Sitch, S., Friedlingstein, P., Smith, W. K., Yuan, W., He, W., Lombardozzi, D., Kautz, M., Zhu, D., Lienert, S., Kato, E., Poulter, B., Sanders, T. G. M., Krüger, I., Wang, R., Zeng, N., Tian, H., Vuichard, N., Jain, A. K., Wiltshire, A., Haverd, V., Goll, D. S., and Peñuelas, J.: Recent global decline of CO₂ fertilization effects on vegetation photosynthesis, Science, 370, 1295–1300, https://doi.org/10.1126/science.abb7772, 2020.

Watson, A. J., Schuster, U., Shutler, J. D., Holding, T., Ashton, I. G. C., Landschützer, P., Woolf, D. K., and Goddijn-Murphy, L.: Revised estimates of ocean-atmosphere CO2 flux are consistent with ocean carbon inventory, Nature Communications, 11, 4422, https://doi.org/10.1038/s41467-020-18203-3, 2020.

Williams, R. G., Ceppi, P., and Katavouta, A.: Controls of the transient climate response to emissions by physical feedbacks, heat uptake and carbon cycling, Environmental Research Letters, 15, 0940c1, https://doi.org/10.1088/1748-9326/ab97c9, 2020.

Yool, A., Palmiéri, J., Jones, C. G., Sellar, A. A., de Mora, L., Kuhlbrodt, T., Popova, E. E., Mulcahy, J. P., Wiltshire, A., Rumbold, S. T., Stringer, M., Hill, R. S. R., Tang, Y., Walton, J., Blaker, A., Nurser, A. J. G., Coward, A. C., Hirschi, J., Woodward, S., Kelley, D. I., Ellis, R., and Rumbold-Jones, S.: Spin-up of UK Earth System Model 1 (UKESM1) for CMIP6, Journal of Advances in Modeling Earth Systems, 12, e2019MS001 933, https://doi.org/https://doi.org/10.1029/2019MS001933, e2019MS001933 10.1029/2019MS001933, 2020.

Zeebe, R. E.: History of Seawater Carbonate Chemistry, Atmospheric CO2, and Ocean Acidification, Annual Review of Earth and Planetary Sciences, 40, 141–165, https://doi.org/10.1146/annurev-earth-042711-105521, 2012.

Zelinka, M. D., Myers, T. A., McCoy, D. T., Po-Chedley, S., Caldwell, P. M., Ceppi, P., Klein, S. A., and Taylor, K. E.: Causes of Higher Climate Sensitivity in CMIP6 Models, Geophysical Research Letters, 47, e2019GL085 782, https://doi.org/https://doi.org/10.1029/2019GL085782, e2019GL085782 10.1029/2019GL085782, 2020.

Ågren, G. I., Wetterstedt, J. A. M., and Billberger, M. F. K.: Nutrient limitation on terrestrial plant growth – modeling the interaction between nitrogen and phosphorus, New Phytologist, 194, 953–960, https://doi.org/https://doi.org/10.1111/j.1469-8137.2012.04116.x, 2012.